Enhancement of performance and stability of thin-film nanocomposite membranes for organic solvent nanofiltration using hypercrosslinked polymer additives

Enhancement of performance and stability of thin-film nanocomposite membranes for organic solvent nanofiltration using hypercrosslinked polymer additives

Hui Zhou[ǂa *], Ammara Akram[ǂb], Andrea Corriea Semiao [b], Richard Malpass-Evans[c], Cher Hon Lau[b,*], Neil B. McKeown[c], Weimin Zhang[a],

[a]School of Water Resources & Environmental Engineering, East China University of Technology, Nanchang 330013, Jiangxi, PR China

[b]School of Engineering, The University of Edinburgh, The King's Buildings, Robert Stevenson Road, EH9 3FB, UK

[c]EaSTCHEM School of Chemistry, The University of Edingburgh, Joseph Black Building, David Brewster Road, EH9 3FJ, UK

Abstract

Hypercrosslinked polymer (HCP) additives were successfully incorporated into two polymer matrices: glassy polymer with intrinsic microporosity comprising ethanoanthracene and Tröger's base (PIM-EA-TB) as well as rubbery polydimethylsiloxane (PDMS), forming thin-film nanocomposite (TFN) membranes for organic solvent nanofiltration (OSN) applications. The thermal stability and surface morphology of TFN membranes were characterized by TGA and SEM. OSN results showed that HCP additives increased the alcohol permeances for both kinds of membranes as it provided extra pathways for alcohol molecules to transport through the membranes. Particularly, the PIM-EA-TB membrane gained above 32% improvement on methanol and ethanol permeances after loading of 5 wt.% HCP, whilst maintaining a rejection of 92% for Rose Bengal. Moreover, the physical aging of PIM-EA-TB membrane was retarded by HCP additives and the swelling of the PDMS membrane in non-polar solvents was reduced. In small quantities, the HCP nanoparticles proved to be effective additives to improve the OSN performances for both glassy and rubbery polymer membranes.

Keywords: Hypercrosslinked polymer; organic solvent nanofiltration; PIM-EA-TB; PDMS; physical aging;

1 Introduction

Organic solvent nanofiltration (OSN) is emerging as a sustainable and effective approach for separating solutes (typical M_w = 200-1000 g·mol^{-1}) from organic media, and has been deployed in pharmaceutical, fine-chemical, biotechnology and petrochemical industry[1-2]. Various polymeric membranes have been studied for OSN, including glassy polyimide (PI)[3], polyamide (PA)[4], polysulfone (PSf)[5], poly[1-(trimethylsilyl)-1-propyne] (PTMSP)[6], polymers with intrinsic microporosity (PIMs)[7] and rubbery poly(dimethylsiloxane) (PDMS)[8]. These membranes are easy to fabricate on low-cost platforms but demonstrate trade-off effects between membrane permeance, rejection and long-term stability which hinder their widespread applications[9]. For instance, thin-film composite membrane comprising a 250 nm thin, dense selective layer of PTMSP deposited on a porous polymer support undergoes a rapid drop in OSN permeance over the first few days due to physical aging[10]. Meanwhile, the benchmark polymer of selective layers in thin-film composite membranes, PDMS, swells extensively in non-polar solvents, limiting their long-term operation[11]. To overcome these limitations, porous nanomaterials such as zeolites[12], polyhedral oligomeric silsesquioxane (POSS)[13], metal-organic frameworks (MOFs)[14] multi-walled carbon nanotubes[15], porous aromatic frameworks (PAFs) and hypercrosslinked polymers (HCPs) have been incorporated into the polymer matrix of the selective layer, yielding thin-film nanocomposite (TFN) membranes with significantly enhanced OSN performances and stability.

Amongst these additives, HCPs offer high surface areas and a convenient synthesis route involving low-cost building blocks and catalysts[16]. Discovered in the 1960s[17], HCPs have since been deployed as ion exchange resins, adsorbents and studied for gas and energy storage and catalysis. The microporosity of HCPs was first exploited to advance the field of membrane separations either as a filler[18, 19], or as a bulk structure[20, 21] with promising potential in gas separation[22], pervaporation[23] and OSN[10]. For example, Hill *et al.*[19, 24] first demonstrated that HCPs could overcome the longstanding issue of physical aging in 100 μm thick PTMSP films whilst increasing the gas separation performances by 50%. Budd *et al.*[25] also

reported the same trends in PIM-1 based composites comprising HCPs fillers. In free-standing HCPs/PTMSP 1.5 μm thin films, Lau and co-workers reported similar permeation enhancement and aging inhibition effect during OSN testing[26]. HCPs demonstrate high potential to simultaneously overcome membrane stability issues that are typically associated with polymer chain mobility such as physical aging and inadequate membrane performances.

Despite its distinctive advantages over other microporous fillers, to date, there are only a handful of studies reporting the use of HCPs in TFN membranes for nanofiltration. For example, Rose *et al.*[27] reported a solvent-responsive nanofiltration membrane by introducing HCPs additives into a PSf dense selective layer of a TFN membrane. The micropores in HCPs were reversibly toggled into an "on" or "off" state by immersion in organic solvents (*iso*-propanol or *n*-pentane) and water. With 40 wt.% HCPs loading, this TFN membrane displayed an *iso*-propanol permeance of 7.01 L m^{-2} h^{-1} bar^{-1} without any rejection towards Rose Bengal (RB), while a lower water permeance of 1.87 L m^{-2} h^{-1} bar^{-1} was observed with a rejection about 52-73% for dyes such as RB, methylene blue, crystal violet and congo red. This pore-toggling capability could be utilized for a new strategy against membrane fouling during nanofiltration. Xie *et al.*[10] recently reported that HCPs could enhance methanol permeances of PTMSP-based TFN membranes by 50% while retarding physical aging of PTMSP by 20%. Clearly, the incorporation of HCPs as additive in ultrathin films can overcome OSN membrane separation performance issues ascribing to polymer chain mobility. However, this has not been demonstrated in PIMs, as well as rubbery polymers such as PDMS where swelling is typically associated with dilation of the polymer layer (mobile polymer chains)[11].

Here we report the preparation of two types of TFN membranes comprising HCP additive dispersed in PIM-EA-TB and PDMS selective layers deposited on porous PAN supports (Fig. 1). PIM-EA-TB[28] comprising Tröger's Base (TB) and ethanoanthracene (EA) units was preferred here over the archetypal PIM, PIM-1[29], for their higher microporosity and greater chain rigidity. PDMS was also chosen as the preferred rubbery polymer matrix as it is the benchmark material deployed in

commercial OSN membranes. The as-prepared TFN membranes demonstrated good alcohol permeances as well as rejection for RB. This study provides an advanced understanding of HCPs interactions with different polymer matrices, representing new material combinations for advanced polymer membranes.

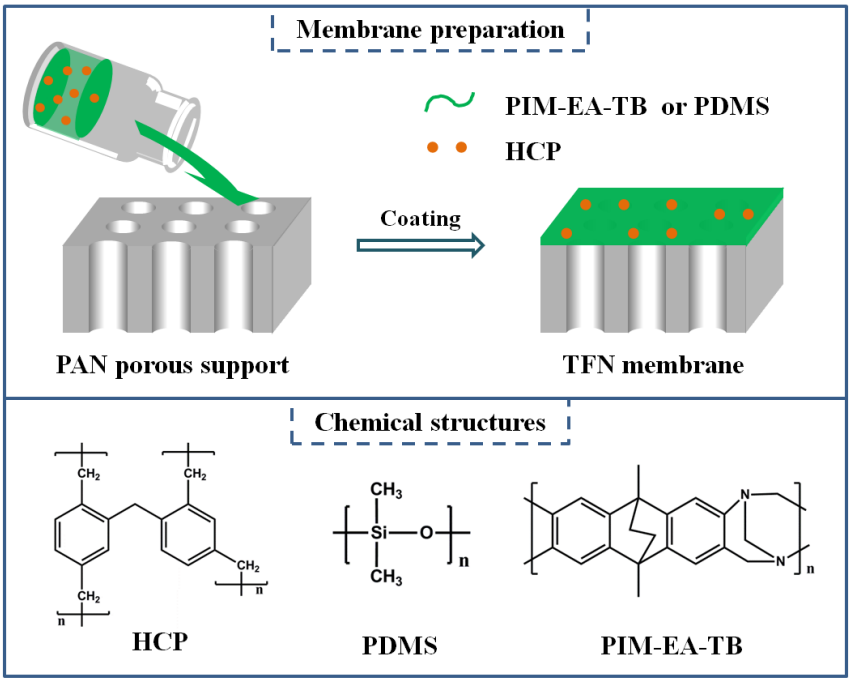

Figure 1. Membrane preparation and chemical structures of membrane materials

2. Experimental

2.1 Materials

Analytical grade methanol, ethanol, *iso*-propanol, *n*-heptane, chloroform, RB (M_w = 1017 g·mol^{-1}), 1,2-dichloroethane (DCE), α,α-dichloro-*p*-xylene (DCX, 98%) and iron(III) chloride were purchased from Sigma-Aldrich and used as received without any further purification. PIM-EA-TB polymer was prepared from the trifluoroacetic acid mediated reaction between dimethoxymethane and 2,6(7)-diamino-9,10-dimethyl -ethanoanthracene as reported[28]. Polydimethylsiloxane (PDMS, type RTV615) in a two-component kit (part A and Part B) was purchased from Momentive Performance Materials, Inc., Germany. The asymmetric polyacrylonitrile (PAN) substrate with the molecular weight cut-off of 20 KDa was purchased from AMI®, USA.

2.2 Synthetic procedure of HCP

The HCP was synthesized according to a literature procedure[19]. Briefly, DCX

monomers (0.076 mol, 13.34 g) was dissolved in anhydrous DCE (90 mL) prior to mixing with a DCE solution (90 mL) of $FeCl_3$ (0.076 mol, 12.35 g). The resulting mixture was stirred in an open vessel at 80 ℃. The precipitated HCP was washed vigorously with water and methanol (until the filtrate was clear) and dried in a vacuum oven at 110 ℃ for 24 h.

2.3 Preparation of membranes

HCP/PIM-EA-TB TFN membranes: The PAN porous support was pretreated by immersion in distilled water at room temperature for 5 h to fill the pores with water, and then quickly wiping off the surface water with a filter paper once removed from water. 1 wt.% PIM-EA-TB was dissolved in chloroform and 5–10 wt. % (with respect to PIM-EA-TB content) HCP was added to this solution. This mixture was stirred for 24 h followed by ultrasonication for 30 min. The mixture was poured and spread over the surface of the pretreated PAN porous supports using a coating knife (Elcometer 3580). Finally, the as-cast membranes were left at room temperature for 24 h before use. Free-standing, dense HCP/PIM-EA-TB films were also fabricated for TGA analysis.

HCP/PDMS TFN membranes: The fabrication protocol of these membranes was largely the same as HCP/PIM-EA-TB TFN membranes, except for the polymers used in the coating solution and the post-treatment thermal protocol. The coating solution was prepared with 10 wt. % PDMS (part A and part B, ratio of 10:1), 5–10 wt. % HCP (with respect to PDMS content) and *n*-heptane. The as-cast membrane was left for 30 min at room temperature to evaporate the solvent and subsequently transferred to a vacuum oven at 90 ℃ overnight for complete curing. Free-standing, dense HCP/PDMS films were fabricated for TGA analysis and membrane swelling test.

2.4 Characterization

The Brunauer-Emmett-Teller (BET) surface area of HCP was determined by nitrogen adsorption-desorption isotherms under 77 K (Quadrasorb-Evo, Quantachrome Corporation, USA). The sample was degassed under vacuum at 120 ℃ for 24 h before characterization.

Dynamic light scattering (DLS) experiments were performed using a Zetasizer

Nano ZS90 (Malvern Instruments, Worcestershire, UK) at room temperature. Solutions were placed in a square glass cuvette. The chemical structure of HCP closely resembles that of polystyrene, hence a refractive index of 1.5865 was chosen for the analysis. The refractive index (1.444) and viscosity (0.5420 mPa·s) of chloroform at 25 ℃ were used.

Thermal gravity analysis (TGA) was performed using a STA 449C Simultaneous Thermal Analyzer (Netzsch Corporation, Germany) over a temperature range of 30 ℃ to 800 ℃, at a heating rate of 5 ℃·min^{-1} with nitrogen flow of 40 mL·min^{-1}. Water contact angle (WCA) measurements were performed on a First Ten Angstroms (FTA 32) instrument. SEM micrographs of HCP particles, surface and cross-section morphologies of TFN membranes were obtained using a JEOS JSM-IT100 Scanning Electron Microscope.

Membrane welling test was carried out by immersing dense HCP/PDMS films in different solvents (ethanol, *iso*-propanol, ethyl acetate and *n*-heptane) at room temperature. The swelling degree was calculated using the masses of the dry and swollen membrane by:

$$\text{Swelling degree} = \frac{W_{swollen} - W_{dry}}{W_{dry}} \times 100\% \quad (1)$$

2.5 Organic solvent nanofiltration

The filtration experiments were carried out at room temperature using a self-made, stainless steel dead-end pressure cell with an effective membrane area of 0.003318 m^2. The chamber above the membrane was filled with about 500 mL feed solution to maintain solute concentration on the same level during the experiment. The feed solution was pressurized with 5–7 bar nitrogen. During filtration, the feed solution was stirred at 700 rpm to avoid concentration polarization. Membrane sample was pre-compacted for 30 min and then permeate (about 5 mL) was collected in capped flasks, weighed, and analyzed. The solvent permeance (P) was calculated using the following equation:

$$P = \frac{W}{\rho A \Delta t \Delta p} \quad (2)$$

where W (g) represents the mass of collected permeate; ρ is the density of solvent; A is the effective membrane area (m^2); Δt is the operation time (h); and Δp is trans-membrane pressure (bar).

The solute rejections of OSNF membranes were calculated using the following equation:

$$R = \left(1 - \frac{C_p}{C_f}\right) \times 100\% \quad (3)$$

where C_p and C_f are the solute concentrations in the permeate and feed solution, respectively. RB concentration in ethanol were measured with a UV−vis Cintra20-GBC apparatus (λ_{max} of RB = 558 nm).

3. Results and discussion

3.1 HCP particles

The HCP particles were synthesized by Friedel-Crafts catalyzed self-condensation of α,α-dichloro-*p*-xylene (DCX). The BET surface area of this HCP was 1233 $m^2\ g^{-1}$ (Fig. 2a). These particles exhibited good thermal stability with a temperature of 5% weight loss ($T_{5\%}$) of 365 ℃ under a nitrogen atmosphere (Fig. 2b). SEM image shows that the HCP has a roughly spherical shape with a diameter of approximately 20 nm (Fig. 2c). DLS indicated that the hydrodynamic diameter (D_h) of HCP particles dispersed in chloroform was approximately 336 nm (Fig. 2d), much larger than the particle size observed from SEM. This could be attributed to both nanoparticle aggregation and swelling[30]. Benzaqui *et al.*[31] reported that the average diameter of ZIF-8 was about 35 nm when measured by SEM, while a D_h of 180 nm in THF was detected by DLS. It is well established that HCPs swell greatly in organic solvents such as toluene, methanol and heptane with volume increasing by a factor of 1.4, 1.4 and 1.5, respectively[32]. The presence of polymers in HCP/chloroform solution further increased the D_h (Fig. 2d). This could be ascribed to the wrapping of polymer chains on the surfaces of HCP aggregates and the formation of HCP/polymer interactions at the expense of interparticle interactions between HCP nanoparticles. The D_h of HCP/PDMS was 166 nm larger than that of HCP/PIM-EA-TB, indicating

greater aggregation of the HCP in PDMS due to the weaker interactions between HCP particles and PDMS chains. The relatively poor compatibility between PDMS and HCP was observed through SEM where HCP particles agglomerated in larger clusters on membrane cross-section, while HCP agglomerations were not observed in HCP/PIM-EA-TB films (Fig. 2e).

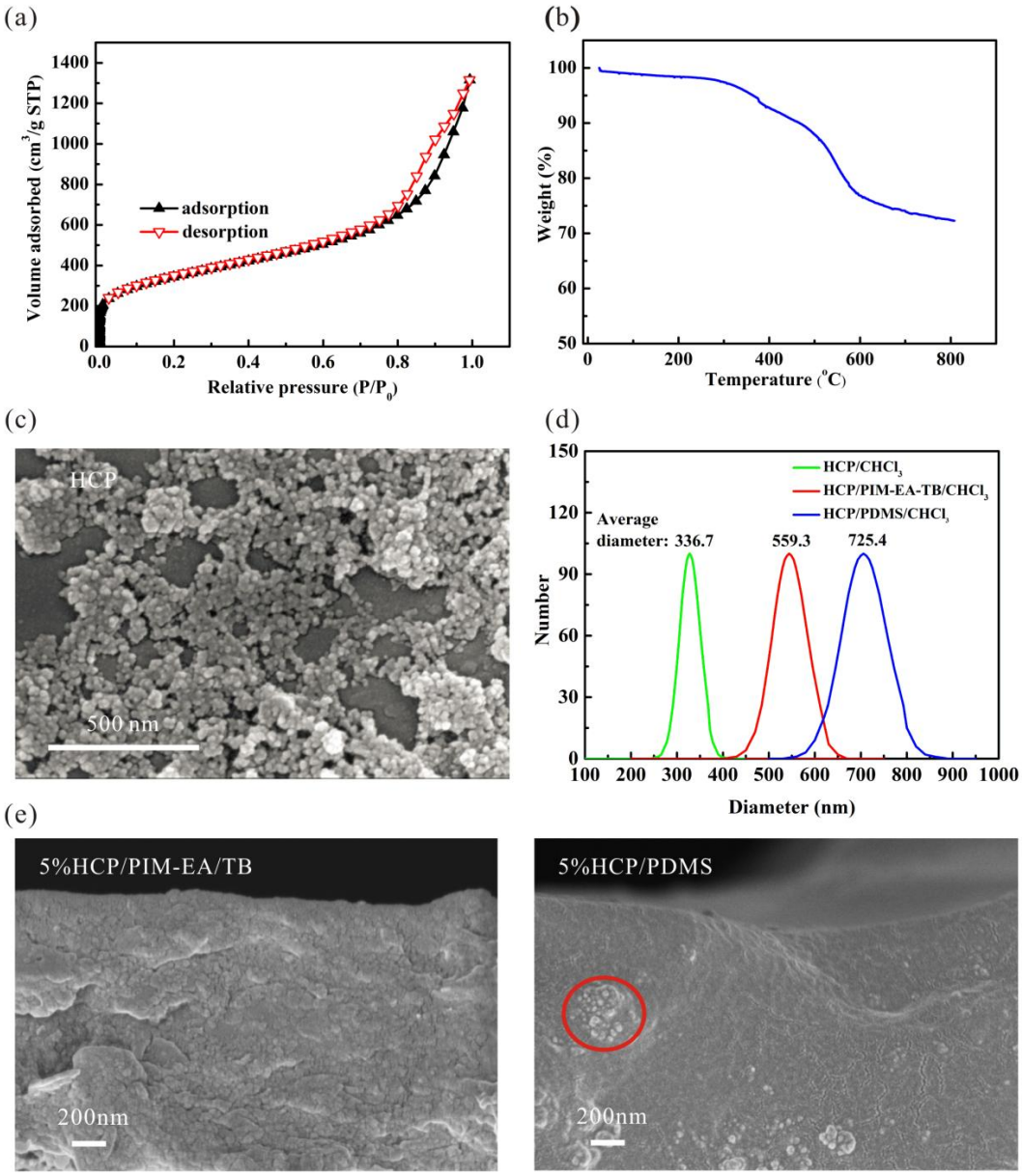

Figure 2. (a) N_2 adsorption isotherm measurements at 77K, (b) TGA curve, (c) SEM image for HCP, (d) HCP particle size distribution by dynamic lighting scattering (DLS) and (e) Cross-section images of TFN membranes with 5 wt.% loading of HCP.

3.2 HCP/PIM-EA-TB membranes

TFN membrane fabrication involved coating a thin selective layer of 5 or 10 wt.% HCP particles dispersed into a PIM-EA-TB matrix onto a porous PAN support. Control TFN membrane with only PIM-EA-TB was also fabricated. The cross-section and surface morphologies of the TFN membranes were examined by SEM (Fig. 3). The PAN porous supports contained finger-like macrovoids in the cross-section and a porous surface with 20-100 nm pores. The cross-section images of the TFN membranes (top row of Fig. 3) revealed a defect-free dense selective layer with a thickness of 600-800 nm that was tightly adhered to the surface of the PAN support with or without HCP. As with other PIM-based membranes[33, 34], round craters could be observed from the top surface of the PIM-EA-TB films deposited on porous supports. The incorporation of HCP into PIM-EA-TB appeared to inhibit the formation of such craters whilst encouraging the formation of ridges. These ridges were enlarged as HCP content increased from 5 to 10 wt.%, possibly due to aggregation of the HCP particles at the surface. HCP additives were dispersed uniformly in the cross-section of the PIM-EA-TB matrix. However, HCP agglomeration, in the form of ridges, could be observed at the surfaces of PIM-EA-TB/HCP TFN membranes (bottom row of Fig. 3).

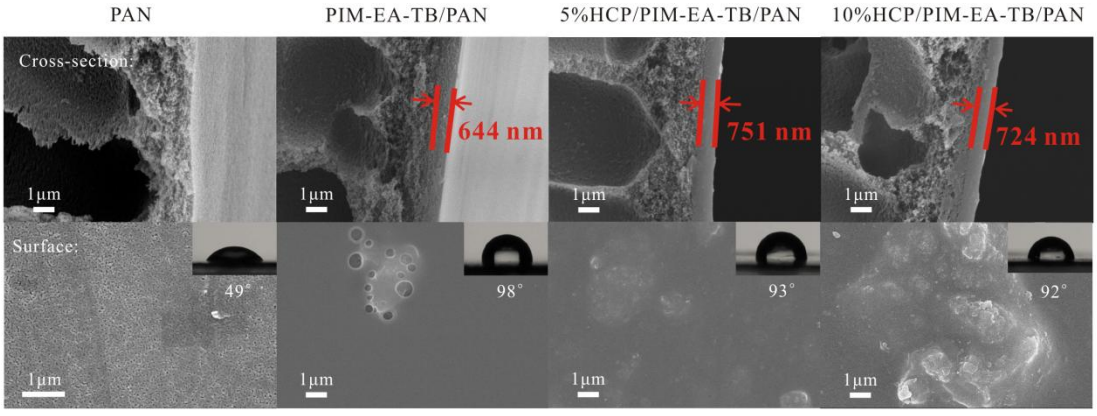

Figure 3. SEM images and WCA of HCP/PIM-EA-TB TFN membranes

The membrane surface can be classified as hydrophobic or hydrophilic if WCA is more than or less than 90 °, respectively. The WCA of PAN porous support layers deployed here was approximately 49 ° indicating a hydrophilic surface (inset of bottom row of Fig. 3). A coating of pristine PIM-EA-TB increased the WCA to 98 °,

transforming hydrophilic PAN supports into hydrophobic PIM-EA-TB/PAN thin-film composites. The addition of HCP additives in PIM-EA-TB matrix reduced the WCAs of resultant TFN membranes, from 98 °to 93-92 °. This slight reduction in WCA might be ascribed to the relatively low WCA of HCP (71 °)[35] compared to PIM-EA-TB. Generally, all of the PIM-EA-TB based TFN membranes can be defined as hydrophobic.

The thermal properties of the HCP/PIM-EA-TB selective layer were investigated by TGA using free-standing, dense membranes. All of the "as-cast" membranes readily released nearly 3% residual solvent (chloroform) under 50 ℃ (Fig. 4). As the membranes were prepared at room temperature to evaporate the solvent, it is possible that some chloroform molecules were trapped in the membranes due to its high affinity towards the Tröger's base groups in PIM-EA-TB[36]. The HCP/PIM-EA-TB membranes presented analogous degradation mechanism to that of pure PIM-EA-TB membrane. Nevertheless, the presence of HCP shifted the $T_{5\%}$ to a slightly higher value for HCP/PIM-EA-TB and generated a higher char yield at 800 ℃.

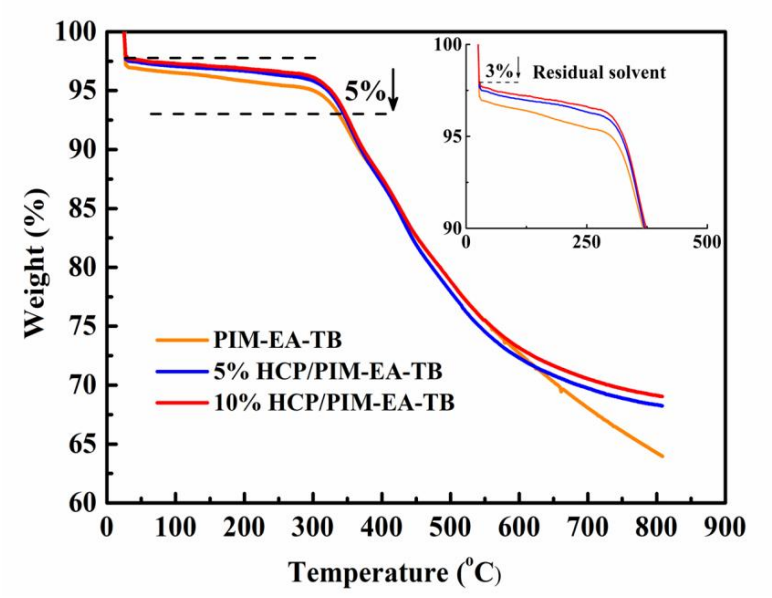

Figure 4. TGA curves of HCP/PIM-EA-TB membranes

The OSN performances of HCP/PIM-EA-TB TFN membranes were measured using a dead-end permeation cell under magnetic stirring at 5 bar. To remove residual solvent from casting, as-cast HCP/PIM-EA-TB based membranes were soaked in methanol for 1 h before OSN characterization[36]. The TFN membranes comprised of

a porous PAN support (MWCO 20 KDa), which shows ethanol permeance of 756 L $m^2h^{-1}bar^{-1}$ and a RB rejection rate of 7%. The deposition of PIM-EA-TB selective layers improved RB rejection rates to 83% at the expense of lower ethanol permeance (2.49 L m^2 h^{-1} bar^{-1}, Fig. 5a). The OSN performances of PIM-EA-TB based TFN membranes were attributed to the skin layer. Fig. 5 shows the OSN performances of PIM-EA-TB based TFN membranes. The pure PIM-EA-TB membrane exhibited initial alcohol permeances in the following order: methanol (5.35 L m^2 h^{-1} bar^{-1}) > ethanol (2.49 L m^2 h^{-1} bar^{-1}) > *iso*-propanol (1.10 L m^2 h^{-1} bar^{-1}). The incorporation of 5 wt.% HCP enhanced initial methanol and ethanol (polar solvents) permeances by 32-36 % and isopropanol (less polar) permeance by 18.7%. This could be ascribed to the intrinsic microporosity of HCP providing additional solvent transportation pathways. The discrepancy in alcohol permeance enhancements was due to the different molecular volume and viscosity of methanol, ethanol and *iso*-propanol[37]. The RB rejection in ethanol for pure PIM-EA-TB TFN membrane was 83%. Although a defect-free dense PIM-EA-TB skin layer was cast on the PAN porous support layer, the surface craters observed by SEM might reduce the rejection of dye. The incorporation of 5 wt.% HCP in the PIM-EA-TB matrix provides a high rejection rate of 92% possibly due to the prevention of crater formation on the membrane surface. However, with 10 wt.% HCP content in PIM-EA-TB where HCP aggregation was apparent from SEM (Fig. 3), the RB rejection rate was reduced to 67%. Additive aggregation could lead to the formation of non-selective voids in the membranes that reduced rejection rate[38].

High free volume polymers such as PIMs are prone to physical aging, especially in thin films [39, 40]. Fig. 5(c) shows that even in the presence of 5 wt.% HCP, the ethanol permeance of PIM-EA-TB based TFN membrane decreased by 47.2% over the first 30 h of continuous operation but then remained stable for further 140 h operation. This initial 47.2% drop in ethanol permeance was lower than the 64.3% loss in ethanol permeance of the pure PIM-EA-TB thin film composite membrane. Carta *et al.*[28] reported that 181 μm thick PIM-EA-TB dense films presented a 20–33% reduction in gas permeabilities on aging. The higher reduction in permeance in this

study was attributed to the thin skin layer, as thin films tend to age much faster than thick ones[40]. Crucially, the ethanol permeance of aged 5 wt.% HCP/PIM-EA-TB TFN membranes were maintained at 1.74 L m^{-2} h^{-1} bar^{-1}, with RB rejection rates above 90 %. This was better than the long-term permeance of the PIM-EA-TB TFN membrane (0.89 L m^{-2} h^{-1} bar^{-1}). Methanol (or ethanol) treatment has been shown previously to reverse the effect of physical aging for highly permeable glassy polymers[41]. For example, this protocol could recover 45% of the ethanol permeance of aged PTMSP membrane that have been exposed to ethanol for 100 h[26]. Here we observed that this permeance recovery protocol had a negligible effect on rejuvenating the collapsed free volume space between PIM-EA-TB polymer chains, particularly in 5 wt.% HCP/PIM-EA-TB composite.

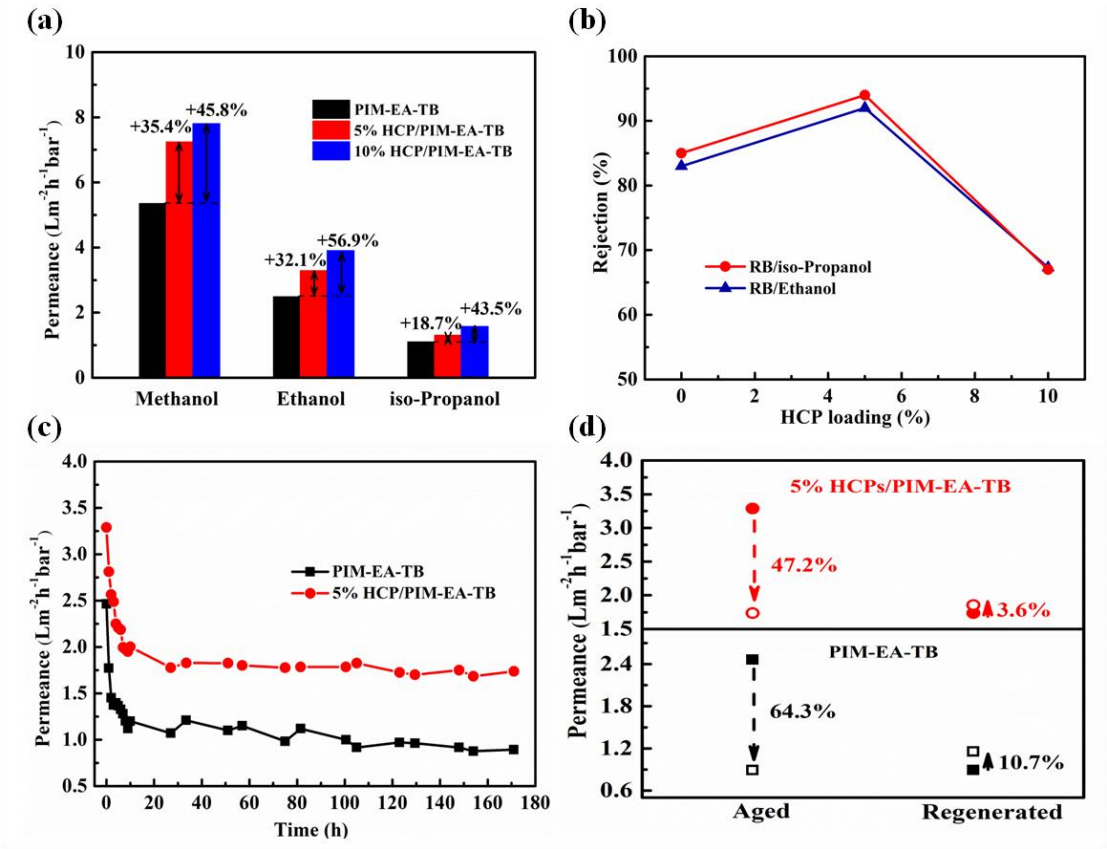

Figure 5. (a) Solvent permeances, (b) RB rejections of HCP/PIM-EA-TB TFN membranes, (c) Long-term operation performance of PIM-EA-TB and 5 wt.% HCP/PIM-EA-TB in ethanol at 5 bar and (d) Change of ethanol permeance after aging (170 h continuous separation) and regenerating (aged membranes soaking in methanol for 7 d under atmosphere).

3.3 HCP/PDMS membranes

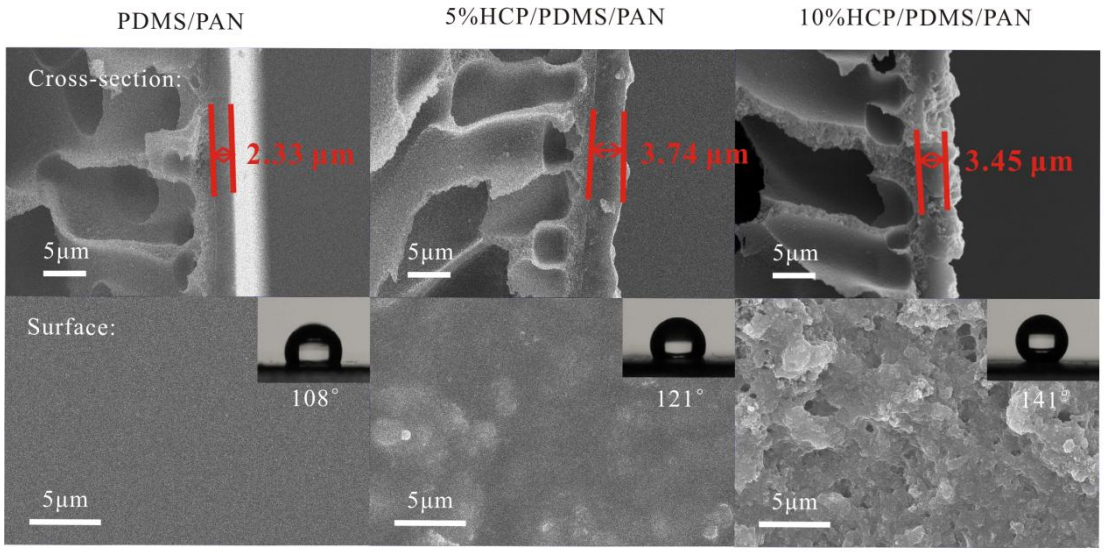

Figure 6. SEM images and WCA of HCP/PDMS TFN membranes

PDMS is the benchmark rubbery material deployed in commercial OSN membranes and therefore it was of interest to study the effect of the HCP additive in PDMS TFN membranes. Fig. 6 shows the cross-section and surface morphologies of HCP/PDMS TFN membranes. The skin-layer thicknesses for all membranes were around 2-4 μm, which were comparable to those of commercial PDMS OSN membranes. The incorporation of HCP seemed to increase the skin-layer thickness possibly due to the change in viscosity of coating solution, while no direct proportional relationship between the thickness and the loading was observed. The surface of the pure PDMS membrane was smooth. As the HCP content increased from 5 to 10 wt.%, the surface of HCP/PDMS TFN membranes became rougher and riddled with pinholes. The WCA of PDMS increased as a function of increasing HCP content (inset of bottom row of Fig. 6). It seems that the incorporation of HCP in PDMS TFN membranes had a different effect on WCA compared to those composed of HCP/PTM-EA-TB. This reverse trend in WCA was caused by the remarkable increase in surface roughness for HCP/PDMS nanocomposites (Fig. 6), due to the poor compatibility between the HCP additive and PDMS matrix. Thus, the highest surface roughness for 10 wt.% HCP/PDMS resulted in the highest WCA of 140 ^{o}C.

Fig. 7a shows that the HCP/PDMS selective layers had a good themal stability, as the $T_{5\%}$ of free-standing membranes were around 420-440 ℃. The swelling behaviors

of PDMS and HCP/PDMS nanocomposites were investigated using different solvents (Fig. 7b). PDMS swelled by 102.1%, 73.4%, 15.8%, 2.1% in the presence of *n*-heptane, ethyl acetate, *iso*-propanol and ethanol, respectively. The embedding of HCP in PDMS matrix decreased the swelling degree of the membrane in *n*-heptane and ethyl acetate. Two factors were responsible for the reduced membrane swelling. Firstly, the HCP additive was not so susceptible to swelling in the two solvents relative to PDMS. Secondly, the PDMS chains near the HCP regions were restrained by interfacial interaction thus suppressing membrane swelling[42]. A comparison of swelling change after incorporation of HCP and other particles into PDMS membrane is also given in Table SI. Interestingly, with HCP, the swelling of PDMS membrane in ethanol and *iso*-propanol increased slightly. This could be ascribed to the relatively high swelling of HCP in these two solvents as compared to that of PDMS.

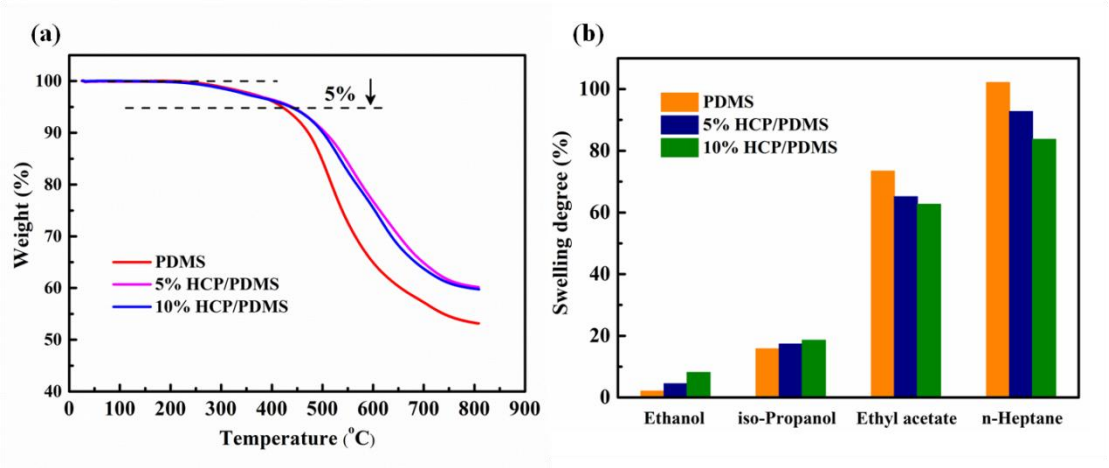

Figure 7. (a) TGA curves and (b) Swelling degrees of HCP/PDMS membranes.

The OSN performance of the PDMS-based TFN membranes for *iso*-propanol and *n*-heptane under 7 bar is shown in Fig. 8. All membranes were soaked in the testing solvent for 24 h to reach a swelling equilibrium before OSN. Pristine PDMS TFN membranes exhibited low permeance towards less polar *iso*-propanol and high permeance towards non-polar *n*-heptane (Fig 8a). This transport property was regulated by HCP additives where *iso*-propanol permeance was enhanced but that for *n*-heptane permeance decreased. These trends of permeance were in accordance with the degree of swelling, as also observed in $Ti_3C_2T_x$ nanosheets filled PDMS membranes[43]. The incorporation of 5 wt.% HCP in PDMS membrane yielded a 34.2 %

improvement in *iso*-propanol permeance with a RB rejection rate of 92%. This enhanced permeability for *iso*-propanol could be attributed to the extra transport pathways provided by the porous HCP additive and the enhanced swelling (Fig. 7b) which caused an expansion of existing transport pores within membrane. Meanwhile, the reduced permeability for n-heptane was mainly due to swelling suppression of the PDMS matrix by the HCP additives, preventing the increase of free volume for solvent transport.

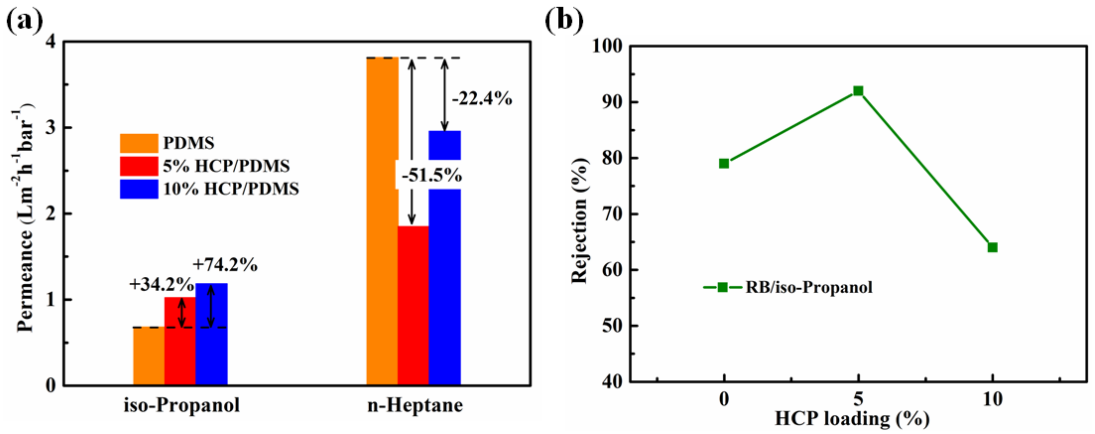

Figure 8. (a) OSN permeances and (b) Rejections of HCP/PDMS TFN membranes under 7 bar.

To better understanding the role of HCP in mixed matrix membranes (MMMs), the mechanisms of interfacial interactions between HCP and polymers were proposed (Figure 9). Two kinds of interactions at the HCP/PIM-EA-TB interface could be possible. One is the intercalation of PIM-EA-TB chains into the porous additive and that chain fixation occurs through the polymer's pendant methyl groups[19, 44-45]. The other one is the sorption of PIM-EA-TB chain on the surface of HCP additives. Owing to the above two interfacial interactions, the HCP/PIM-EA-TB exhibited good compatibility resulting in the absence of HCP aggregation on the cross-section of membrane, and the anti-aging effect of HCP in PIM-EA-TB matrix.

Figure 2e suggested that HCP and PDMS were not as compatible as HCP with PIM-EA-TB as agglomerations of HCP could be observed in the PDMS matrix. Hence, for HCP/PDMS there could be potentially only one form of interaction, most likely the sorption of PDMS chain on the surface of HCP additives. This could be due to expulsion of PDMS's pendant methyl groups that were most likely to be adsorbed

within HCP pores initially during coating (as per PIM-EA-TB, PIM-1 and PTMSP). When the solvent evaporated, the flexible PDMS chains folded effectively and the swollen HCP shrank, potentially forcing the methyl group out from HCP pores. Hence, relatively poor compatibility between HCP and flexible PDMS chains was presented.

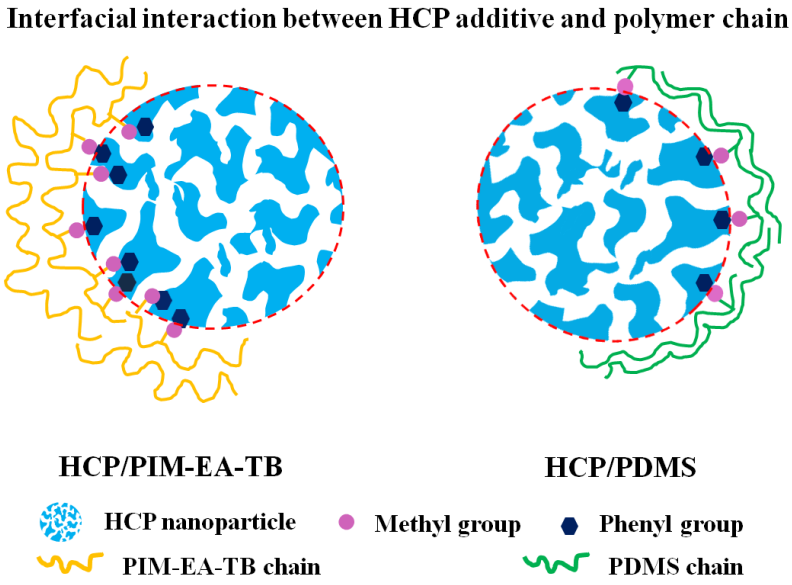

Figure 9. The schematic diagram for mechanisms of interfacial interactions between HCP and glassy PIM-EA-TB or rubbery PDMS polymer

A comparison of OSN performances of TFN membranes prepared in this study and other membranes from literatures is shown in Fig. 9. The 5 wt.% HCP loaded PDMS or PIM-EA-TB membranes exhibited higher *iso*-propanol permeances with a moderate rejections to RB, compared to PEEK[46, 47] and mixed matrix membranes containing porous additives such as $Cu_3(BTC)_2$[48], ZIF-8[49] or POSS[13]. Besides, the ethanol permeance of 5% HCP/PIM-EA-TB membrane surpassed that of membranes like sPPSU[50], UiO-66/PI[51], crosslinked PIM-1[52], and ZIF-8/PES[48], and was comparable to POSS/PDA[13] and PA/PI[53] membranes with a satisfactory retention of RB.

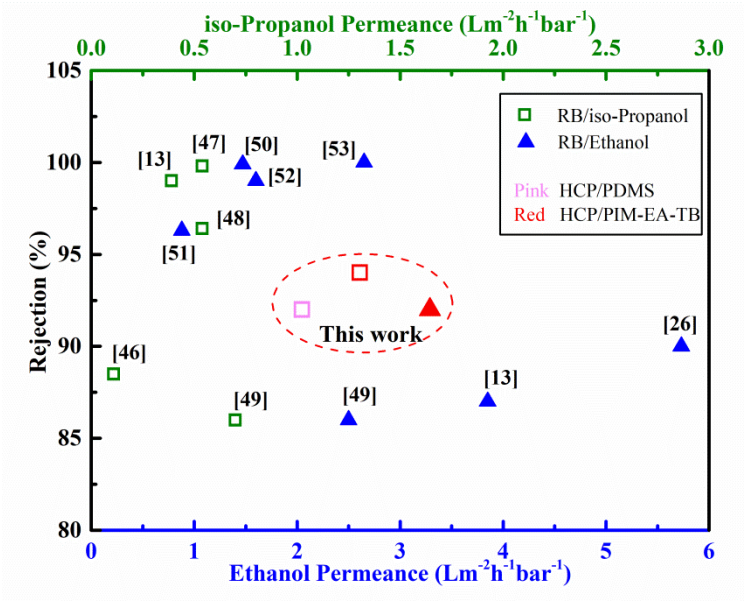

Figure 10. Comparison of the HCP filled TFN membranes in this study with other membranes in OSN separation of IPA/RB or EtOH/RB mixture. (POSS/PDA[13], PEEK[46], PEEKWC[47], $Cu_3(BTC)_2$/PDMS[48], ZIF-8/PES[49], HCP/PTMSP[26], sPPSU[50], UiO-66/PI[51], Crosslinked-PIM[52], PA/PI[53])

3. Conclusions

In summary, we reported the performance of two types of OSN TFN membranes by incorporating HCP particles into a high free volume glassy polymer (PIM-EA-TB) and a standard rubbery polymer (PDMS). The porous HCP particles facilitated the transport of alcohol molecules and enhanced alcohol permeances. Both TFN membranes acquired better OSN performance for alcohol solvents with 5 wt.% HCP loading. Different enhancement effects were observed for these two types of membranes despite using the same additive, and possible interfacial interactions between HCP additives and glassy/rubbery polymer were proposed. Interactions between PDMS chains and HCP additives were most likely due to relatively weak sorption mechanisms that led to poor compatibility between the additives and polymer matrix. Hence, HCP agglomerated within the cross-section of HCP/PDMS membranes. The lack of HCP aggregates within PIM-EA-TB matrix was indicative of better compatibility between these materials, and most probably due to the sorption of PIM chains on HCP surfaces and intercalation of PIM chains within HCP pores.

Combined, these mechanisms were key for the observed aging mitigation effect of HCP in PIM-EA-TB matrix. Overall, the addition of a small amount of HCP particles improves the OSNF performances for both glassy and elastic polymer membranes.

Acknowledgements

This study was financially supported by National Natural Science Foundation of China (Grant No. 42174091 and 41964003) and Jiangxi Provincial Natural Science Foundation (Grant No. 20202BAB201013).

References

[1] M.H.D.A. Farahani, D. Ma, P.N. Ardakani, Nanocomposite membranes for organic solvent nanofiltration, Separation & Purification Reviews, 49 (2018) 177-206.

[2] K. Ge, Q. Liu, J. Deng, D. Nobes, Y. Wang, Y. Wang, X. Chen, Rock magnetic investigation and its geological significance for vein-type uranium deposits in southern China. Geochemistry, Geophysics, Geosystems, 18 (2017) 1333-1349.

[3] C. Li, S. Li, L. Lv, B. Su, M.Z. Hu, High solvent-resistant and integrally crosslinked polyimide-based composite membranes for organic solvent nanofiltration, Journal of Membrane Science, 564 (2018) 10-21.

[4] S. Karan, Z. Jiang, A.G. Livingston, Sub–10 nm polyamide nanofilms with ultrafast solvent transport for molecular separation, Science, 348 (2015) 1347-1351.

[5] A.K. Hołda, B. Aernouts, W. Saeys, I.F.J. Vankelecom, Study of polymer concentration and evaporation time as phase inversion parameters for polysulfone-based SRNF membranes, Journal of Membrane Science, 442 (2013) 196-205.

[6] A.V. Volkov, V.V. Parashchuk, D.F. Stamatialis, V.S. Khotimsky, V.V. Volkov, M. Wessling, High permeable PTMSP/PAN composite membranes for solvent nanofiltration, Journal of Membrane Science, 333 (2009) 88-93.

[7] J. Li, M. Zhang, W. Feng, L. Zhu, L. Zhang, PIM-1 pore-filled thin film composite membranes for tunable organic solvent nanofiltration, Journal of Membrane Science, 601 (2020) 117951.

[8] D. Zedel, A. Drews, M. Kraume, Retention of surfactants by organic solvent nanofiltration and influences on organic solvent flux, Separation and Purification Technology, 158 (2016) 396-408.

[9] Y. Cao, X. Chen, S. Feng, Y. Wan, J. Luo, Nanofiltration for decolorization: membrane fabrication, applications and challenges. Industrial & Engineering Chemistry Research, 59 (2020) 19858-19875.

[10] Q. Liu, S.J.D. Smith, K. Konstas, D. Ng, K. Zhang, M.R. Hill, Z. Xie, Construction of ultrathin PTMSP/Porous nanoadditives membranes for highly efficient organic solvent nanofiltration (OSN), Journal of Membrane Science, 620 (2021) 118911.

[11] E.J. Kappert, M.J.T. Raaijmakers, K. Tempelman, F.P. Cuperus, W. Ogieglo, N.E. Benes, Swelling of 9 polymers commonly employed for solvent-resistant nanofiltration membranes: A comprehensive dataset, Journal of Membrane Science, 569 (2019) 177-199.

[12] L.E.M. Gevers, I.F.J. Vankelecom, P.A. Jacobs, Solvent-resistant nanofiltration with filled polydimethylsiloxane (PDMS) membranes, Journal of Membrane Science, 278 (2006) 199-204.

[13] Y.C. Xu, Y.P. Tang, L.F. Liu, Z.H. Guo, L. Shao, Nanocomposite organic solvent nanofiltration

membranes by a highly-efficient mussel-inspired co-deposition strategy, Journal of Membrane Science, 526 (2017) 32-42.
[14] S. Sorribas, P. Gorgojo, C. Tél lez, J. Coronas, A.G. Livingston, High flux thin film nanocomposite membranes based on metal–organic frameworks for organic solvent nanofiltration, Journal of the American Chemical Society, 135 (2013) 15201-15208.
[15] M.H.D.A. Farahani, D. Hua, T.-S. Chung, Cross-linked mixed matrix membranes (MMMs) consisting of amine-functionalized multi-walled carbon nanotubes and P84 polyimide for organic solvent nanofiltration (OSN) with enhanced flux, Journal of Membrane Science, 548 (2018) 319-331.
[16] L. Tan, B. Tan, Hypercrosslinked porous polymer materials: design, synthesis, and applications, Chemical Society reviews, 46 (2017) 3322-3356.
[17] V.A. Davankov, S.V. Rogozhin, M.P. Tsyurupa, USSR Pat., 299165 (1969).
[18] J. Hradil, P. Sysel, L. Brožová, J. Kovářová, J. Kotek, Heterogeneous membranes based on a composite of a hypercrosslinked microparticle adsorbent and polyimide binder, Reactive and Functional Polymers, 67 (2007) 432-441.
[19] C.H. Lau, X. Mulet, K. Konstas, C.M. Doherty, M.A. Sani, F. Separovic, M.R. Hill, C.D. Wood, Hypercrosslinked additives for ageless gas-separation membranes, Angewandte Chemie, 55 (2016) 1998-2001.
[20] Z.-A. Qiao, S.-H. Chai, K. Nelson, Z. Bi, J. Chen, S.M. Mahurin, X. Zhu, S. Dai, Polymeric molecular sieve membranes via in situ cross-linking of non-porous polymer membrane templates, Nature Communications, 5 (2014) 1-8.
[21] A. Chinnappan, W.-J. Chung, H. Kim, Hypercross-linked microporous polymeric ionic liquid membranes: synthesis, properties and their application in H_2 generation, Journal of Materials Chemistry A, 45 (2015) 22960-22968.
[22] R. Hou, R. O'Loughlin, J. Ackroyd, Q. Liu, C.M. Doherty, H. Wang, M.R. Hill, S.J.D. Smith, Greatly enhanced gas selectivity in mixed-matrix membranes through size-controlled hyper-cross-linked polymer additives, Industrial & Engineering Chemistry Research, 59 (2020) 13773-13782.
[23] X.Q. Cheng, K. Konstas, C.M. Doherty, C.D. Wood, X. Mulet, Z. Xie, D. Ng, M.R. Hill, C.H. Lau, L. Shao, Organic microporous nanofillers with unique alcohol affinity for superior ethanol recovery toward sustainable biofuels, ChemSusChem, 10 (2017) 1887-1891.
[24] C.H. Lau, K. Konstas, A.W. Thornton, A.C.Y. Liu, S. Mudie, D.F. Kennedy, S.C. Howard, A.J. Hill, M.R. Hill, Gas-separation membranes loaded with porous aromatic frameworks that improve with age, Angewandte Chemie International Edition, 54 (2015) 2669-2673.
[25] R.S. Bhavsar, T. Mitra, D.J. Adams, A.I. Cooper, P.M. Budd, Ultrahigh-permeance PIM-1 based thin film nanocomposite membranes on PAN supports for CO2 separation, Journal of Membrane Science, 564 (2018) 878-886.
[26] X.Q. Cheng, K. Konstas, C.M. Doherty, C.D. Wood, X. Mulet, Z. Xie, D. Ng, M.R. Hill, L. Shao, C.H. Lau, Hyper-cross-linked additives that impede aging and enhance permeability in thin polyacetylene films for organic solvent nanofiltration, ACS applied materials & interfaces, 9 (2017) 14401-14408.
[27] K. Schute, F. Jansen, M. Rose, Solvent-responsive and switchable nanofiltration membranes based on hypercrosslinked polymers with permanent porosity, ChemNanoMat, 4 (2018) 562-567.
[28] M. Carta, R. Malpass-Evans, M. Croad, Y. Rogan, J.C. Jansen, P. Bernardo, F. Bazzarelli, N.B. McKeown, An efficient polymer molecular sieve for membrane gas separations, Science, 339 (2013)

303-307.
[29] K. Pilnáček, O. Vopička, M. Lanč, M. Dendisová, M. Zgažar, P.M. Budd, M. Carta, R. Malpass-Evans, N.B. McKeown, K. Friess, Aging of polymers of intrinsic microporosity tracked by methanol vapour permeation, Journal of Membrane Science, 520 (2016) 895-906.
[30] Q. Li, Z. Zhan, S. Jin, B. Tan, Wettable magnetic hypercrosslinked microporous nanoparticle as an efficient adsorbent for water treatment, Chemical Engineering Journal, 326 (2017) 109-116.
[31] M. Benzaqui, R. Semino, N. Menguy, F. Carn, T. Kundu, J.M. Guigner, N.B. McKeown, K.J. Msayib, M. Carta, R. Malpass-Evans, C. Le Guillouzer, G. Clet, N.A. Ramsahye, C. Serre, G. Maurin, N. Steunou, Toward an understanding of the microstructure and interfacial properties of PIMs/ZIF-8 mixed matrix membranes, ACS Appllied Materials & Interfaces, 8 (2016) 27311-27321.
[32] M.P. Tsyurupa, V.A. Davankov, Hypercrosslinked polymers: basic principle of preparing the new class of polymeric materials, Reactive and Functional Polymers, 53 (2002) 193-203.
[33] M. Cook, P.R.J. Gaffney, L.G. Peeva, A.G. Livingston, Roll-to-roll dip coating of three different PIMs for organic solvent nanofiltration, Journal of Membrane Science, 558 (2018) 52-63.
[34] D. Fritsch, P. Merten, K. Heinrich, M. Lazar, M. Priske, High performance organic solvent nanofiltration membranes: development and thorough testing of thin film composite membranes made of polymers of intrinsic microporosity (PIMs), Journal of Membrane Science, 401 (2012) 222-231.
[35] X. Wang, H. Li, J. Huang, Adsorption of p-chlorophenol on three amino-modified hyper-cross-linked resins, Journal of Colloid and Interface Science, 505 (2017) 585-592.
[36] E. Tocci, L. D. Lorenzo, P. Bernardo, G. Clarizia, F. Bazzarelli, N.B. McKeown, M. Carta, R. Malpass-Evans, K. Friess, K. Pilnáček, M. Lanč, Y.P. Yampolskii, L. Strarannikova, V. Shantarovich, M. Mauri, J.C. Jansen, Molecular modeling and gas permeation properties of a polymer of intrinsic microporosity composed of ethanoanthracene and tröger's base units, Macromolecules, 47 (2014) 7900-7916.
[37] M.H. Abdellah, C.A. Scholes, B.D. Freeman, L. Liu, S.E. Kentish, Transport of terpenes through composite PDMS/PAN solvent resistant nanofiltration membranes, Separation and Purification Technology, 207 (2018) 470-476.
[38] E.L. Butler, C. Petit, A.G. Livingston, Poly(piperazine trimesamide) thin film nanocomposite membrane formation based on MIL-101: filler aggregation and interfacial polymerization dynamics, Journal of Membrane Science, 596 (2020) 117482.
[39] P. Gorgojo, S. Karan, H.C. Wong, M.F. Jimenez-Solomon, J.T. Cabral, A.G. Livingston, Ultrathin polymer films with intrinsic microporosity: anomalous solvent permeation and high flux membranes, Advanced Functional Materials, 24 (2014) 4729-4737.
[40] Y. Huang, D.R. Paul, Physical aging of thin glassy polymer films monitored by gas permeability, Polymer, 45 (2004) 8377-8393.
[41] P.M. Budd, N.B. McKeown, B.S. Ghanem, K.J. Msayib, D. Fritsch, L. Starannikova, N. Belov, O. Sanfirova, Y. Yampolskii, V. Shantarovich, Gas permeation parameters and other physicochemical properties of a polymer of intrinsic microporosity: polybenzodioxane PIM-1, Journal of Membrane Science, 325 (2008) 851-860.
[42] L. Wang, X. Han, J. Li, X. Zhan, J. Chen, Hydrophobic nano-silica/polydimethylsiloxane membrane for dimethylcarbonate–methanol separation via pervaporation, Chemical Engineering Journal, 171 (2011) 1035-1044.
[43] X. Wu, L. Hao, J. Zhang, X. Zhang, J. Wang, J. Liu, Polymer-$Ti_3C_2T_x$ composite membranes to overcome the trade-off in solvent resistant nanofiltration for alcohol-based system, Journal of

Membrane Science, 515 (2016) 175-188.
[44] R. Hou, S.J.D. Smith, C.D. Wood, R.J. Mulder, C.H. Lau, H. Wang, and M.R. Hill, Solvation effects on the permeation and aging performance of PIM-1-based MMMs for gas separation, ACS Applied Materials & Interfaces, 11 (2019) 6502-6511.
[45] C.H. Lau, K. Konstas, C.M. Doherty, S.J.D. Smith, R. Hou, H. Wang, M. Carta, H. Yoon, J. Park, B.D. Freeman, R. Malpass-Evans, E. Lasseuguette, M. Ferrari, N.B. McKeown, M.R. Hill, Tailoring molecular interactions between microporous polymers in high performance mixed matrix membranes for gas separations, Nanoscale, 12 (2020) 17405-17410.
[46]K. Hendrix, M. V. Eynde, G. Koeckelberghs, I.F.J. Vankelecom, Crosslinking of modified poly(ether ether ketone) membranes for use in solvent resistant nanofiltration, Journal of Membrane Science, 447 (2013) 212-221.
[47] M.G. Buonomenna, G. Golemme, J.C. Jansen, S.H. Choi, Asymmetric PEEKWC membranes for treatment of organic solvent solutions, Journal of Membrane Science, 368 (2011) 144-149.
[48] S. Basu, M. Maes, A. Cano-Odena, L. Alaerts, D.E.D. Vos, I.F.J. Vankelecom, Solvent resistant nanofiltration (SRNF) membranes based on metal-organic frameworks, Journal of Membrane Science, 344 (2009) 190-198.
[49] Y. Li, L.H. Wee, A. Volodin, J.A. Martens, I.F.J. Vankelecom, Polymer supported ZIF-8 membranes prepared via an interfacial synthesis method, Chemical Communications, 51 (2015) 918-920.
[50] A.A. Tashvigh, L. Luo, T.-S. Chung, M. Weber, C. Maletzko, A novel ionically cross-linked sulfonated polyphenylsulfone (sPPSU) membrane for organic solvent nanofiltration (OSN), Journal of Membrane Science, 545 (2018) 221-228.
[51] D. Ma, G. Han, Z.F. Gao, S.B. Chen, Continuous UiO-66-type metal–organic framework thin film on polymeric support for organic solvent nanofiltration, ACS Applied Materials & Interfaces, 11 (2019) 45290-45300.
[52] J. Gao, S. Japip, T.-S. Chung, Organic solvent resistant membranes made from a cross-linked functionalized polymer with intrinsic microporosity (PIM) containing thioamide groups, Chemical Engineering Journal, 353 (2018) 689-698.
[53] S. Hermans, E. Dom, H. Mariën, G. Koeckelberghs, I.F.J. Vankelecom, Efficient synthesis of interfacially polymerized membranes for solvent resistant nanofiltration, Journal of Membrane Science, 476 (2015) 356-363.